INELASTIC ANALYSIS OF METALLIC STRUCTURES IN THE PRESENCE OF THERMAL GRADIENTS USING NEWER CONSTITUTIVE RELATIONS

Virendra Kumar and Subrata Mukherjee

ERDA Report No: COO-2733-3

February 1976

Deaprtment of Theoretical and Applied Mechanics

Cornell University

Ithaca, N.Y. 14853

CONTRACT NO. E(11-1)-2733

DISCLAIMER

ABSTRACT

Several newer constitutive relations have recently been proposed for describing the mechanical behavior of metals and alloys under elevated temperature creep conditions. A salient feature of the mathematical structure of many of these relations is that they typically express the nonelastic strain rates as functions of the current values of stress, temperature and some other suitably defined state variables. A computational scheme is presented in this paper for the inelastic analysis of metallic structures subjected to both mechanical and thermal loadings and obeying constitutive relations of the type described above. Several numerical examples for the creep of thick-walled spheres, cylinders and rotating discs in the presence of thermal gradients are presented. The particular constitutive relations used in these calculations are due to Hart. The proposed computational scheme is found to be very efficient from the view point of both computational time and effort. The effects of previous cold work on the stress redistribution and creep of these structural elements are discussed.

INTRODUCTION

The numerous technological applications of metals and alloys at elevated temperatures have prompted in recent years a great amount of research interest in the area of their high temperature inelastic behavior. This growth of interest has led to a remarkable effort in the development of constitutive relations for modelling this high temperature inelastic behavior of metals which is known to be a time dependent phenomenan, highly nonlinear and hereditary in nature. The classical theories of creep [1,2] currently in use are found to have serious drawbacks [3,4,5]. For example, the strain hardening and time hardening theories do not take into account the effect of prior deformation history on subsequent creep behavior and are incapable of representing a softening of the material which accompanies creep recovery. A variety of newer constitutive relations [6-11] have recently been proposed in order to overcome the shortcomings of classical theories and represent more faithfully the mechanical behavior of metals at elevated temperatures, especially under conditions of complex time dependent mechanical and thermal loadings.

A salient feature of the mathematical structure of these newer constitutive relations [6-11] is that the nonelastic strain rates are expressed as functions of the current values of stress, temperature and certain well defined state variables. These state variable evolve with deformation according to certain laws in such a way that their rates of change with time are again functions of stress, temperature and these state variables. Thus, according to these constitutive relations, the current values of stress, temperature and some state variables uniquely determine the nonelastic strain rates and the rates of change of these

state variables with time. This particular mathematical feature of these equations leads to a very simple and efficient method of three-dimensional inelastic analysis of structures which we shall describe presently. It is important to note that the mathematical structure of classical creep theories also fit into this general format if the time independent plastic strain in the sense of classical plasticity is ignored. No such restriction is necessary if any of these newer theories is used because they treat the so called time independent strain of classical plasticity and time dependent creep strain of classical theories as a single quantity called permanent strain which is regarded as time dependent.

In this paper we present a general computational technique for three-dimensional inelastic analysis of structures made of materials that obey constitutive relations of the type described above and subjected to both mechanical and thermal loadings. The method is illustrated for thick-walled spheres, cylinders and rotating discs under steady internal and external pressures and radial temperature gradients. The constitutive relations due of Hart [7,8] are employed to obtain the numerical results for these problems. The numerical results presented are discussed in the context of Hart's theory and the computational scheme, and very encouraging conclusions are drawn.

As described in the following section, Hart's theory has a sound experimental basis for many metals and alloys under uniaxial loading [12-19]. A novel feature of this theory is its ability to differentiate in a simple way between geometrically identical specimens with different initial deformation states, e.g. between annealed and cold worked specimens. In regard to multiaxial stress conditions, the present

authors recently analyzed the problem of creep of thick cylinders under internal and external pressures using Hart's theory [20] in the absence of thermal gradients. Certain simplifying assumptions that were made in [21] are relaxed in the present paper and more general loading situations are considered. The numerical solutions presented in this paper are extremely important from the viewpoint of validation of any general purpose finite element code which may later be developed using the proposed computational method and Hart's theory.

1. BRIEF REVIEW OF HART'S THEORY

In this section we present a brief outline of Hart's theory. A detailed description can be found in references [6-8].

We shall concentrate our attention on the constitutive laws governing grain matrix deformation. For situations under consideration the contribution due to grain boundary sliding is neglible and is, therefore, not included in the present formulation of Hart's theory [7]. The accumulated total strain due to grain matrix deformation, ϵ, at any time can be decomposed into four components:

$$\epsilon = \epsilon^e + \epsilon^a + \epsilon^p + \epsilon^T \tag{1.1}$$

where ϵ^e is the elastic strain which is related to stress by Hooke's law; ϵ^a is the anelastic strain, a stored strain that is completely recoverable eventually upon unloading; ϵ^p is the completely irrecoverable and path dependent permanent strain; and ϵ^T is the thermal strain. The anelastic strain rate $\dot{\epsilon}^a$ is appreciable for relatively short times following abrupt changes of load and plays a very important role in nonmonotonic loading. In case of relatively steady loading, however, we

can use the transient free relationship in which $\dot{\epsilon}^a \approx 0$. In this paper we consider only steady loading situations so that the anelastic strain ϵ^a is ignored. Thus ϵ is the sum of ϵ^e, ϵ^p and ϵ^T. It should be pointed out that ϵ^p represents the completely irrecoverable component of strain and includes the time independent as well as the time dependent plastic strains in a classical sense.

Hart, Li and their coworkers have performed experiments on various metals and alloys at different temperatures [12-19]. They have concluded that the rate of permanent strain for these materials at any time is given by the current values of the stress σ, temperature T and a single state variable σ^* called hardness. The hardness characterizes the present deformation state of the material and differentiates between geometrically identical specimens with different initial deformation states e.g. between annealed and cold worked specimens. The hardness at time t depends upon the deformation history upto time t and increases with the amount of cold work. They have also demonstrated that for all the materials tested the growth rate of hardness $\dot{\sigma}^*$ is a function of σ, σ^* and T only. Based upon these experiments, Hart has proposed the following constitutive equations for steady loading conditions

$$\dot{\epsilon}^p = A(\sigma,\sigma^*,T) = (\sigma^*/G)^m f \exp(-Q/RT)\phi(\sigma/\sigma^*) \tag{1.2}$$

$$\dot{\sigma}^* = B(\sigma,\sigma^*,T) = \dot{\epsilon}^p \sigma^* \Gamma(\sigma,\sigma^*) \tag{1.3}$$

In the above f is an arbitrary coefficient with dimensions of frequency, R is the gas constant, G is the isothermal modulus of rigidity and is a function of temperature, m is a material constant with a value between 3 and 8, Q is a measure of thermal activation energy and is a function

of temperature alone, T is temperature (in °K) and ϕ and Γ are measured functions of their arguments. Note that unlike classical plasticity there is no yield stress here and that the current values of σ, σ^* and T uniquely determine $\dot{\epsilon}^p$ and $\dot{\sigma}^*$.

The three dimensional generalization is made by Hart in keeping with concepts of incremental plasticity. Two invariants are defined as

$$\sigma = \sqrt{(3/2)s_{ij}s_{ij}} \quad , \quad \dot{\epsilon}^p = \sqrt{(2/3)\dot{\epsilon}^p_{ij}\dot{\epsilon}^p_{ij}} \tag{1.4}$$

where $s_{ij} = \sigma_{ij} - (1/3)\sigma_{kk}\delta_{ij}$ is the deviatoric stress tensor. As usual, a repeated index implies summation over that index and δ_{ij} is the Kronicker delta. It is now assumed that these invariants σ and $\dot{\epsilon}^p$ are related to each other through the scalar hardness σ^* according to (1.2) and (1.3). Finally, a flow rule relating the permanent strain rate tensor to the deviatoric stress tensor is postulated as

$$\dot{\epsilon}^p_{ij} = \frac{3}{2}\left(\frac{\dot{\epsilon}^p}{\sigma}\right)s_{ij} = \frac{3}{2}\frac{A(\sigma,\sigma^*,T)}{\sigma}s_{ij} \tag{1.5}$$

Equations (1.2) - (1.5) constitute Hart's theory for relatively steady multiaxial loading. For nonmonotonic loading conditions constitutive equations including ϵ^a must be used. These are given in [8].

2. GENERAL METHOD OF THREE DIMENSIONAL INELASTIC ANALYSIS

We now present a general computational method for analysis of three dimensional creep problems which is motivated by expressing the governing differential equations of the problem in terms of rates as follows:

Kinematic: $$\dot{\underset{\sim}{\epsilon}} = \dot{\underset{\sim}{\epsilon}}^e + \dot{\underset{\sim}{\epsilon}}^p + \dot{\underset{\sim}{\epsilon}}^T = (\underset{\sim}{\nabla}\dot{u} + \dot{u}\underset{\sim}{\nabla})/2 \tag{2.1}$$

or equivalently, compatibility of total strain rates

$$\nabla \times \dot{\varepsilon} \times \nabla = \dot{\varepsilon}_{ij,k\ell} + \dot{\varepsilon}_{k\ell,ij} - \dot{\varepsilon}_{ik,j\ell} - \dot{\varepsilon}_{j\ell,ik} = 0 \qquad (2.2)$$

Equilibrium: $$\nabla \cdot \dot{\sigma} + \dot{F} = 0 \qquad (2.3)$$

Constitutive: $$\dot{\varepsilon}^e = (\dot{\sigma} - \frac{\nu}{1+\nu}\Theta I)/2G \qquad (2.4)$$

$$\dot{\varepsilon}^p = \frac{3}{2}(\frac{\dot{\varepsilon}^p}{\sigma})s = \frac{3}{2}\frac{A(\sigma,\sigma^*,T)}{\sigma}s \qquad (2.5)$$

$$\dot{\varepsilon}^T = \alpha \dot{T} I \qquad (2.6)$$

$$\dot{\sigma}^* = B(\sigma,\sigma^*,T) \qquad (2.7)$$

In the above u is the displacement, ∇ the gradient operator, F the body force per unit volume, ν the Poisson's ratio, α the coefficient of linear thermal expansion, $\Theta = \mathrm{tr}\sigma = \sigma_{kk}$, and I the unit tensor. The dot denotes differentiation with respect to time.

a. Stress rate formulation

The compatibility equation (2.2) can be written as

$$\nabla \times \dot{\varepsilon}^e \times \nabla = -\nabla \times \dot{\varepsilon}^p \times \nabla - \nabla \times \dot{\varepsilon}^T \times \nabla \qquad (2.8)$$

We now replace the strain rates from the constitutive equations (2.4)-(2.6) to get

$$\nabla \times [\frac{1}{2G}(\dot{\sigma} - \frac{\nu}{1+\nu}\Theta I)] \times \nabla = -\nabla \times [\frac{3}{2}\frac{A(\sigma,\sigma^*,T)}{\sigma}s] \times \nabla - \nabla \times [\alpha \dot{T} I] \times \nabla \qquad (2.9)$$

The traction boundary condition is

$$\dot{\underset{\sim}{\sigma}} \cdot \underset{\sim}{n} = \dot{\underset{\sim}{T}} \tag{2.10}$$

where $\underset{\sim}{n}$ is the unit outward normal to the boundary and $\underset{\sim}{T}$ the prescribed surface traction vector. The traction is assumed to be a continuous function of time so that its rate is defined everywhere. If discontinuous loading functions are involved, the constitutive realtions including anelastic strains [8] must be used and elastic unloading must be taken into consideration. Since in this paper we only consider relatively steady processes, we shall not elaborate further on this point.

The initial conditions are obtained by specifying the initial distribution of hardness and by taking the initial permanent strains to be zero. Since $\underset{\sim}{\epsilon}^p = 0$ at $t = 0$, the stresses and strains at $t = 0$ are given by the corresponding thermoelastic solution of the problem. Thus

$$\underset{\sim}{\sigma}(\underset{\sim}{x},0) = \underset{\sim}{\sigma}^o(\underset{\sim}{x}), \quad \underset{\sim}{\epsilon}^o(\underset{\sim}{x},0) = \underset{\sim}{\epsilon}^e(x,0) + \underset{\sim}{\epsilon}^T(\underset{\sim}{x},0)$$

$$\underset{\sim}{\epsilon}^p(\underset{\sim}{x},0) = 0, \quad \sigma^*(\underset{\sim}{x},0) = \sigma_o^*(\underset{\sim}{x}) \tag{2.11}$$

where $\underset{\sim}{\sigma}^o(\underset{\sim}{x})$ and $\underset{\sim}{\epsilon}^o(\underset{\sim}{x})$ correspond to the thermoelastic solution at $t = 0$. In other words, $\underset{\sim}{\sigma}^o$, $\underset{\sim}{\epsilon}^o$ are obtained by solving the following problem:

$$\underset{\sim}{\epsilon}^o = \frac{1}{2G}(\underset{\sim}{\sigma}^o - \frac{\nu}{1+\nu}\Theta^o \underset{\sim}{I}) + \alpha T^o \underset{\sim}{I} \tag{2112}$$

$$\underset{\sim}{\nabla} \times [\frac{1}{2G}(\underset{\sim}{\sigma}^o - \frac{\nu}{1+\nu}\Theta^o \underset{\sim}{I}] \times \underset{\sim}{\nabla} + \underset{\sim}{\nabla} \times [\alpha T^o \underset{\sim}{I}] \times \underset{\sim}{\nabla} = 0 \tag{2.13}$$

$$\underset{\sim}{\nabla} \cdot \underset{\sim}{\sigma}^o = -\underset{\sim}{F}^o \ , \quad \underset{\sim}{\sigma}^o \cdot \underset{\sim}{n} = \underset{\sim}{T}^o \tag{2.14}$$

In the above, T^o, $\underset{\sim}{F}^o$ and $\underset{\sim}{\tau}^o$ are the temperature, body force and traction distributions, respectively at $t = 0$. $\sigma^*(\underset{\sim}{x},0)$ would usually be uniform throughout the material, but nonuniform initial hardness may be introduced during fabrication of the structure.

b. Displacement rate formulation

In this case we write the equilibrium equation (2.3) in terms of displacement rates using (2.1), (2.4-2.6) to get

$$\nabla^2 \dot{\underset{\sim}{u}} + \frac{1}{1-2\nu} \nabla\nabla \cdot \dot{\underset{\sim}{u}} = -\frac{\dot{\underset{\sim}{F}}}{G} + 2\nabla \cdot \left[\frac{3}{2} \frac{A(\sigma,\sigma^*,T)}{\sigma} \underset{\sim}{s}\right] + \frac{2(1+\nu)}{(1-2\nu)} \nabla(\alpha \dot{T}) \tag{2.15}$$

The corresponding displacement boundary condition is

$$\dot{\underset{\sim}{u}} = \dot{\underset{\sim}{\Delta}} \tag{2.16}$$

where $\underset{\sim}{\Delta}$ is the prescribed displacement vector on the surface of the body. Once again we assume Δ to be a continuous function of time. The initial conditions are obtained in a manner similar to the stress rate formulation case.

The observation to be made here is that the resulting boundary value problem in rates for both of the above cases is linear and has the same structure as the linear thermoelastic boundary value problem except for an inhomogeneous term on the right which is uniquely determined by the current values of σ, σ^* and T. Thus, stress or displacement rates at any time are obtained by solving a linear boundary value problem similar to classical thermoelasticity. This forms the basis of the computational method proposed.

c. Computational scheme

The initial stresses and strains are first obtained by solving the corresponding thermoelastic problem. Thus, $\underset{\sim}{\sigma}^{o}$ and $\bar{\sigma}_{o}^{*}$ are known. The temperature history is assumed to be prescribed in advance.

Case a. The stress and hardness rates at $t = 0$ are obtained by solving the set of linear, inhomogeneous partial differential equations (2.3), (2.9) and (2.7) subject to the boundary condition (2.10).

Case b. The displacement and hardness rates at $t = 0$ are obtained by solving (2.15) and (2.7) subject to the boundary condition (2.16). The total strain rate is now obtained from $\dot{\underset{\sim}{\varepsilon}} = (\nabla\dot{\underset{\sim}{u}} + \dot{\underset{\sim}{u}}\nabla)/2$ and the permanent and thermal strain rates from (2.5) and (2.6). Now $\dot{\varepsilon}^{e}$ is obtained by substracting $\dot{\varepsilon}^{p}$ and $\dot{\varepsilon}^{T}$ from $\dot{\varepsilon}$ and the stress rates from the inverted form of Hooke's Law (2.4).

The stresses and hardness are obtained at a new time Δt by using, for example, Euler's method $(\underset{\sim}{\sigma}|_{\Delta t} = \underset{\sim}{\sigma}^{o} + \dot{\underset{\sim}{\sigma}}|_{t=0} \times \Delta t$ etc.) or higher order integration methods such as the fourth-order Runge-Kutta method. These new stresses and hardness are now used to obtain the rates at time Δt and so on, and the process continued upto the desired final time. Thus, knowing the stress and hardness at time t, the rates at time t are obtained by solving the appropriate boundary value problem. These rates are then used to update the stress and hardness to the time $t + \Delta t$ by using a suitable integration scheme. It should be pointed out that the boundary value problem (2.3), (2.9), (2.10)(or, equivalently, (2.15)-(2.16)) may have to be solved by finite difference or finite element methods for complicated problems. In such cases, the corresponding thermoelastic problem at zero time may also require use of finite difference or finite

element methods. Choice of time step Δt is found to be very crucial in the computation and must be small initially because the rates are usually high in the beginning.

We have restricted case a to traction and case b to displacement boundary value problems merely for ease of presentation. Sometimes it is convenient to use case b (with (2.16) suitably modified) for traction boundary value problems. Mixed boundary value problems must be handled on a problem by problem basis.

The computational scheme is described above in the context of Hart's theory. However, as mentioned earlier, the method is quite general and can be readily extended to other constitutive relations by suitably modifying equations (2.5) and (2.7).

3. ILLUSTRATIVE EXAMPLES

In this section we present formulations for boundary value problems involving spheres, cylinders and rotating discs. The loads and temperatures are assumed steady throughout.

(a) Sphere under internal and external pressures.

We consider a thick-walled sphere of internal radius a and external radius b subjected to steady internal and external presssures p and q respectively (see Fig. 1a). The inside temperature is T_a and the outside temperature T_b, both being invariant in time. Because of spherical symmetry, the only nonzero component of displacement is the radial displacement u which is a function of the radius r and time. The nonzero components of stress and strain, σ_r, $\sigma_\theta = \sigma_\phi$, ϵ_r and $\epsilon_\theta = \epsilon_\phi$, are functions of r and t only. The usual notation is used and the subscripts r, θ and ϕ denote the radial and two mutually

orthogonal circumferential directions.

The governing differential equations take the form

Kinematic: $$\epsilon_r = \frac{\partial u}{\partial r} , \quad \epsilon_\theta = \epsilon_\phi = \frac{u}{r} \tag{3.1}$$

Equilibrium: $$\frac{\partial \sigma_r}{\partial r} + \frac{2(\sigma_r - \sigma_\theta)}{r} = 0 \tag{3.2}$$

Constitutive: $$\epsilon_r = (\sigma_r - 2\nu\sigma_\theta)/E + \epsilon_r^p + \alpha T \tag{3.3}$$

$$\epsilon_\theta = ((1-\nu)\sigma_\theta - \nu\sigma_r)/E + \epsilon_\theta^p + \alpha T \tag{3.4}$$

$$\dot{\epsilon}_r^p = (\dot{\epsilon}^p/\sigma)(\sigma_r - \sigma_\theta) , \tag{3.5}$$

$$\dot{\epsilon}_\theta^p = \dot{\epsilon}_\phi^p = (\dot{\epsilon}^p/2\sigma)(\sigma_\theta - \sigma_r) \tag{3.6}$$

In the above E is Young's Modulus. To this we must add Hart's constitutive equations (1.2) and (1.3).

The boundary conditions are given by

$$\sigma_r(a,t) = -p , \quad \sigma_r(b,t) = -q \tag{3.7}$$

$$T(a,t) = T_a , \quad T(b,t) = T_b \tag{3.8}$$

The initial conditions are given by

$$\sigma^*(r,0) = \sigma_o^*(r) \tag{3.9}$$

together with the zero time thermoelastic solution to the problem given in the appendix A.

Using the displacement rate formulation outlined in section 2b, we can obtain the displacement rates and then the stress rates. These are

$$\dot{\sigma}_r = \left(\frac{E}{1-\nu}\right)\left\{\int_a^r \frac{\dot{\epsilon}^p_r}{\eta}\,d\eta - \frac{(r^3-a^3)}{(b^3-a^3)}\frac{b^3}{r^3}\int_a^b \frac{\dot{\epsilon}^p_r}{\eta}\,d\eta\right\} \tag{3.10}$$

$$\dot{\sigma}_\theta = \left(\frac{E}{1-\nu}\right)\left\{\int_a^r \frac{\dot{\epsilon}^p_r}{\eta}\,d\eta - \frac{(2r^3+a^3)}{2(b^3-a^3)}\frac{b^3}{r^3}\int_a^p \frac{\dot{\epsilon}^p_r}{\eta}\,d\eta + \frac{\dot{\epsilon}^p_r}{2}\right\} \tag{3.11}$$

The problem can now be solved by using the computational scheme outlined in Section 2c.

(b) Cylinder with internal and external pressures and axial load.

We consider a long thick walled cylinder of internal and external radii a and b subjected to internal and external pressures p and q respectively and an axial force P (see Fig. 1a,b). The inside and outside temperatures are T_a and T_b respectively and the pressures p and q and the temperature, T_a and T_b are invariant in time. The end effects are neglected and the solution is assumed valid sufficiently far from the ends. Plane cross sections are assumed to remain plane. Under these assumptions, and because of cylindrical symmetry, the tangential displacement component u_θ vanishes and the radial displacement u_r is a function of r and t only. The nonvanishing stresses and strains are σ_r, σ_θ, σ_z, ϵ_r, ϵ_θ and ϵ_z, with ϵ_z a function of t only and the others functions of r and t. The usual cylindrical coordinates are used with r, θ and z denoting the radial, tangential and axial directions respectively.

The governing differential equations take the form:

Kinematic: $$\epsilon_r = \frac{\partial u_r}{\partial r} \quad , \quad \epsilon_\theta = \frac{u_r}{r} \quad , \quad \epsilon_z = \frac{\partial u_z}{\partial z} \tag{3.12}$$

Equilibrium: $$\frac{\partial \sigma_r}{\partial r} + \frac{(\sigma_r - \sigma_\theta)}{r} = 0 \tag{3.13}$$

$$\int_a^b 2\pi r \sigma_z dr = P \tag{3.14}$$

Constitutive: $$\epsilon_r = (\sigma_r - \nu(\sigma_\theta + \sigma_z))/E + \epsilon_r^p + \alpha T \tag{3.15}$$

$$\epsilon_\theta = (\sigma_\theta - \nu(\sigma_r + \sigma_z)/E + \epsilon_\theta^p + \alpha T \tag{3.16}$$

$$\epsilon_z = (\sigma_z - \nu(\sigma_r + \sigma_\theta))/E + \epsilon_z^p + \alpha T \tag{3.17}$$

$$\dot{\epsilon}_r^p = (\dot{\epsilon}^p/2\sigma)(2\sigma_r - \sigma_\theta - \sigma_z) \tag{3.18}$$

$$\dot{\epsilon}_\theta^p = (\dot{\epsilon}^p/2\sigma)(2\sigma_\theta - \sigma_r - \sigma_z) \tag{3.19}$$

$$\dot{\epsilon}_z^p = (\dot{\epsilon}^p/2\sigma)(2\sigma_z - \sigma_r - \sigma_\theta) \tag{3.20}$$

To this we must add Hart's constitutive equations (1.2) and (1.3). The boundary conditions have the same form as (3.7) and (3.8). The initial hardness distribution must be specified as in (3.9) and the initial stresses and strains are obtained from the thermoelastic solution given in the appendix A.

Using the displacement rate formulation outlined in Section 2b, we can obtain the displacement and then the stress rates. These are

$$\dot{\sigma}_r = \frac{E}{2(1-\nu^2)}\left\{\int_a^r \frac{(\dot{\epsilon}_r^p-\dot{\epsilon}_\theta^p)}{\eta}\,d\eta - \frac{(r^2-a^2)}{(b^2-a^2)}\frac{b^2}{r^2}\int_a^b \frac{(\dot{\epsilon}_r^p-\dot{\epsilon}_\theta^p)}{\eta}\,d\eta\right\}$$

$$+ \frac{E(1-2\nu)}{2(1-\nu^2)}\frac{1}{r^2}\left\{\int_a^r \eta\dot{\epsilon}_z^p d\eta - \frac{(r^2-a^2)}{(b^2-a^2)}\int_a^b \eta\dot{\epsilon}_z^p d\eta\right\} \qquad (3.21)$$

$$\dot{\sigma}_\theta = \frac{E}{2(1-\nu^2)}\left\{\int_a^r \frac{(\dot{\epsilon}_r^p-\dot{\epsilon}_\theta^p)}{\eta}\,d\eta - \frac{(r^2+a^2)}{(b^2-a^2)}\frac{b^2}{r^2}\int_a^b \frac{(\dot{\epsilon}_r^p-\dot{\epsilon}_\theta^p}{\eta}\,d\eta\right\}$$

$$- \frac{E(1-2\nu)}{2(1-\nu^2)}\frac{1}{r^2}\left\{\int_a^r \eta\dot{\epsilon}_z^p d\eta + \frac{(r^2+a^2)}{(b^2-a^2)}\int_a^b \eta\dot{\epsilon}_z^p d\eta\right\} - \frac{E}{(1-\nu^2)}\{\dot{\epsilon}_\theta^p+\nu\dot{\epsilon}_z^p\} \qquad (3.22)$$

$$\dot{\sigma}_z = \frac{E\nu}{(1-\nu^2)}\left\{\int_a^r \frac{(\dot{\epsilon}_r^p-\dot{\epsilon}_\theta^p)}{\eta}\,d\eta - \frac{b^2}{(b^2-a^2)}\int_a^b \frac{(\dot{\epsilon}_r^p-\dot{\epsilon}_\theta^p)}{\eta}\,d\eta\right\}$$

$$+ \frac{E(2-\nu)}{(1-\nu^2)}\frac{1}{(b^2-a^2)}\int_a^b \eta\dot{\epsilon}_z^p d\eta + \frac{E}{(1-\nu^2)}\{\nu\dot{\epsilon}_r^p-(1-\nu)\dot{\epsilon}_z^p\} \qquad (3.23)$$

The problem can now be solved by using the computational scheme outlined in Section 2c. The plane strain case ($\epsilon_z=0$) is given in Appendix B.

(c) Rotating disc.

We next consider a thin, uniform, circular disc of internal and external radii a and b, thickness h, rotating with a constant angular velocity ω about its axis of symmetry (see Fig. 1c). The inside curved surface is traction free and the outside curved surface is considered subjected to a steady radial peripheral stress q to simulate the effect of blade loading. The inside and outside temperatures are T_a and

T_b respectively and are invariant in time. Plane stress conditions are assumed to prevail so that the axial stress σ_z is zero. Under these assumptions, and because of axial symmetry, u_θ vanishes and u_r is a function of r and t only. The nonvanishing stresses and strains, σ_r, σ_θ, ϵ_r, ϵ_θ and ϵ_z, are functions of r and t only. The mass density of the disc material is ρ.

The governing differential equations take the form

Kinematic:
$$\epsilon_r = \frac{\partial u}{\partial r} , \quad \epsilon_\theta = \frac{u}{r} \tag{3.24}$$

Equilibrium:
$$\frac{\partial \sigma_r}{\partial r} + \frac{(\sigma_r - \sigma_\theta)}{r} + \rho\omega^2 r = 0 \tag{3.25}$$

Constitutive:
$$\epsilon_r = (\sigma_r - \nu\sigma_\theta)/E + \epsilon_r^p + \alpha T \tag{3.26}$$

$$\epsilon_\theta = (\sigma_\theta - \nu\sigma_r)/E + \epsilon_\theta^p + \alpha T \tag{3.27}$$

$$\epsilon_z = -\nu(\sigma_r + \sigma_\theta)/E + \epsilon_z^p + \alpha T \tag{3.28}$$

$$\dot{\epsilon}_r^p = (\dot{\epsilon}^p/2\sigma)(2\sigma_r - \sigma_\theta) \tag{3.29}$$

$$\dot{\epsilon}_\theta^p = (\dot{\epsilon}^p/2\sigma)(2\sigma_\theta - \sigma_r) \tag{3.30}$$

$$\dot{\epsilon}_z^p = -(\dot{\epsilon}^p/2\sigma)(\sigma_r + \sigma_\theta) \tag{3.31}$$

As usual we must also include Hart's constitutive equations (1.2) and (1.3).

The boundary conditions for the stresses are

$$\sigma_r(a,t) = 0 , \quad \sigma_r(b,t) = q \tag{3.32}$$

and those for temperature are of the form (3.8). The initial hardness distribution must be specified as in (3.9) and the initial stresses and strains are obtained from the thermoelastic solution given in the appendix A.

Using the displacement rate formulation outlined in section 2b we can obtain the displacement and then the stress rates. These are

$$\dot{\sigma}_r = \frac{E}{2}\left\{\int_a^r \frac{(\dot{\epsilon}_r^p-\dot{\epsilon}_\theta^p)}{\eta}\,d\eta - \frac{(r^2-a^2)}{(b^2-a^2)}\frac{b^2}{r^2}\int_a^b \frac{(\dot{\epsilon}_r^p-\dot{\epsilon}_\theta^p)}{\eta}\,d\eta\right\}$$

$$+ \frac{E}{2r^2}\left\{\int_a^r \eta\dot{\epsilon}_z^p d\eta - \frac{(r^2-a^2)}{(b^2-a^2)}\int_a^b \eta\dot{\epsilon}_z^p d\eta\right\} \qquad (3.33)$$

$$\dot{\sigma}_\theta = \frac{E}{2}\left\{\int_a^r \frac{(\dot{\epsilon}_r^p-\dot{\epsilon}_\theta^p}{\eta}\,d\eta - \frac{(r^2+a^2)}{(b^2-a^2)}\frac{b^2}{r^2}\int_a^b \frac{(\dot{\epsilon}_r^p-\dot{\epsilon}_\theta^p)}{\eta}\,d\eta\right\}$$

$$- \frac{E}{2r^2}\left\{\int_a^r \eta\dot{\epsilon}_z^p d\eta + \frac{(r^2+a^2)}{(b^2-a^2)}\int_a^b \eta\dot{\epsilon}_z^p d\eta\right\} - E\dot{\epsilon}_\theta^p \qquad (3.34)$$

$$\dot{\epsilon}_z = -\left\{\int_a^r \frac{(\dot{\epsilon}_r^p-\dot{\epsilon}_\theta^p)}{\eta}\,d\eta - \frac{b^2}{(b^2-a^2)}\int_a^b \frac{(\dot{\epsilon}_r^p-\dot{\epsilon}_\theta^p)}{\eta}\,d\eta\right\}$$

$$+ \frac{\nu}{(b^2-a^2)}\int_a^b \eta\dot{\epsilon}_z^p d\eta + \dot{\epsilon}_z^p + \nu\dot{\epsilon}_\theta^p \qquad (3.35)$$

The change of disc thickness is governed by

$$\dot{h} = h\dot{\epsilon}_z \qquad (3.36)$$

and the problem can be solved by using the computational scheme outlined in Section 2c.

4. NUMERICAL RESULTS AND DISCUSSION

Results of numerical calculations carried out for a sphere, cylinder and rotating disc are presented in this section, The particular alloy chosen is 1100 Aluminum for which data were obtained by Ellis, Wire and Li [19]. For 1100 Aluminum alloy, equations (1.2) and (1.3) assume the special forms

$$\dot{\epsilon}^p = (\sigma^*/G)^m f \exp(-Q/RT)[\ell n(\sigma^*/\sigma)]^{-1/\lambda} \tag{4.1}$$

$$\dot{\sigma}^* = \dot{\epsilon}^p \sigma^* \Lambda(\sigma/G)^{\delta}(\sigma^*/G)^{-\beta} \tag{4.2}$$

where $m = 5$, $\lambda = 0.11$, $\delta = 7.82$, $\beta = 12.5$, $\Lambda = 4 \times 10^{-11}$, $f = 2.613 \times 10^{21} sec^{-1}$, $G = 3.234 \times 10^6$ psi(2.230×10^4 M Pa) at 482°F (250°C), (reference 21), $Q = 1.326 \times 10^5$ Btu. k mole^{-1}(1.404×10^5k J·k mole^{-1}), $R = 4.36297$ Btu. k mole^{-1}.°R^{-1}(8.31434 k J·k mole^{-1}, °K^{-1}). In the above equations, σ and σ^* are in units of psi (or M Pa) and t is in seconds. The value of Q here is equal to the activation energy for atomic self diffusion at 482° F (250°C). Equations (4.1) and (4.2) are valid for $\sigma^* > \sigma$ (the case where $\sigma^* < \sigma$ is discussed in [8]). Other parameters required for the thermoelastic (zero time) solution are $\nu = .358$, $\alpha = 14.22 \times 10^{-6}$ °F^{-1} (25.6×10^{-6}°C^{-1}), $\rho = .098$ ℓbm/in^3(2.712×10^3 kg/m^3).

The appropriate equations are nondimensionalized through the use of the following dimensionless variables

$$\bar{\gamma} = \gamma/p \tag{4.3}$$

where γ stands for any variable having the dimensions of stress, e.g. σ_r, σ_θ, σ_z, σ^*, σ, q, or G, and

$$\xi = r/a \ , \quad \kappa = b/a \ , \quad \bar{u} = u/a \ , \quad \bar{h} = h/a. \qquad (4.4)$$

For the rotating disc problem, we use $\rho\omega^2 a^2$ instead of the internal pressure p in (4.3).

Numerical calculations have been carried out for a cylinder (Figs. 2-4), sphere (Figs. 5-7) and rotating disc (Figs. 8-10) made of 1100 Aluminum alloy. In all cases with thermal gradient the inside temperature T_a is 482°F (250°C) and the outside temperature T_b is 437°F (225°C). In Figs. 8b and 9b we also show the uniform temperature case with $T_a = T_b = 482°F$ (250°C). The internal pressure p for the cylinder is 1000 psi (6.895 M Pa) and the axial load $P = \pi(a^2 p - b^2 q)$ to simulate a closed ended cylinder. The internal pressure for the sphere is 1500 psi (10.342 M Pa) except in Fig. 6 where creep at several different pressures is shown. The external pressure q is taken to be zero in all cases. The angular speed of the disc is 10,000 rpm (ω = 1047.2 rad/s). The values for pressure, angular speed and temperature are chosen such that the mechanical and therml stresses at zero time are of comparable magnitude. Several different distributions of the initial hardness $\sigma_o^*(r)$ are considered.

The Runge-Kutta method of order four has been used for integrating forward in time and the trapezoidal rule has been used to evaluate the spatial integrals appearing in the relevant equations. The radii ratio κ for the cylinder and sphere is 2 and the dimensionless shell thickness κ-1 has been divided into 50 equal segments for these numerical calculations. In case of the disc $\kappa = 3$, and κ-1 has been divided into 100 equal

segments. The computations have been carried out on an IBM 370/168 computer.

Figures 2a, 3a and 4a show the redistribution of radial, tangential and axial stresses in the cylinder during creep. The stress changes rapidly in the beginning and this process slows down considerably as time proceeds. After 100 hours, the stress distributions become almost invariant in time.

The effect of initial hardness on stress relaxation is shown in Figs. 2b, 3b and 4b. The initial hardness level characterizes the initial state of a specimen and is determined by its previous mechanical and thermal history. We compare two different uniformly hardened cases, one lightly cold worked and the other with 10% cold work [19]. We observe, as expected, that the stresses in the softer cylinder relax faster than in the hardened cylinder. The effect of initial hardness on the stresses at long times is, however, found to be negligible.

Figure 5 shows similar results for a spherical shell. This time we compare an uniformly hardened (10% cold worked) sphere with another that is hardened inside and soft outside. The hardness distribution in the latter case is assumed to be given by $\bar{\sigma}_o^*(\xi) = 2\bar{\sigma}(\xi,0)$. The stresses relax much more rapidly in the softer sphere and in this case the long time value of the stresses are affected by the initial hardness distribution.

The effect of pressure and hardness on creep is shown in Fig. 6. The creep of the inner radius of the sphere is shown for four different cases. For the same pressure (1500 psi i.e. 10.342 M Pa) the softer sphere (III) creeps more than a sphere with more cold work (IV). The highly nonlinear effect of the internal pressure can be seen by comparing the curves I, II

and IV all of which represent the same hardness (10% cold work). Similar curves were obtained by the authors in [20] for a cylinder with no thermal gradient.

In all cases where the initial hardness is assumed uniform in space, the structural elements harden but the change of hardness is too small to be evident within the plotting accuracy. This is a consequence of the fact that the initial hardness level in these cases is such that $\dot{\bar{\sigma}}^*$ in (4.2) is very small. However, for the sphere with variable initial hardness ($\bar{\sigma}_o^*(\xi) = 2\bar{\sigma}(\xi,0)$), we find (Fig. 7) that appreciable hardening occurs and the rate of hardening, as expected, slows with time.

Figs. 8 and 9 show stress redistribution in a rotating disc with and without thermal gradient. Once again the initial uniform hardness level represents 10% cold work. The same general characteristics as in the cases of the cylinder and sphere are observed. Note that since the initial mechanical and thermal stresses are of comparable magnitude, the spatial distributions of stresses with and without thermal gradient are considerably different.

Fig. 10 shows creep of the inside and outside radii and the change of disc thickness $\Delta\bar{h}$ with time in the presence of a thermal gradient. Outward radial creep is accompanied by thinning of the disc since the inelastic portion of the deformation is assumed to be incompressible.

Choice of time step is very crucial in the computation and variable time steps are necessary. The initial time steps must be small because the rates are higher in the beginning. The computational scheme is very efficient. Typical computing time for the results presented in Figs. 8-10 for the rotating disc, for example, is approximately 40 seconds on an IBM 370/168.

5. CONCLUSIONS

In this paper we have presented a very efficient computational scheme for analysis of inelastic behavior of structures composed of metals and alloys which obey a broad class of newer constitutive relations. Several numerical examples for spheres, cylinders and rotating discs in the presence of thermal gradients are presented. These results are very important from the viewpoint of checking any general purpose finite element code that might be developed in the future for these newer constitutive relations.

Hart's theory of inelastic deformation gives promising results for the multiaxial problems analyzed here. The ability to distinguish rather easily between different initial states is a novel feature of this theory. There are indications that the extended version of this theory including anelastic strains [8] will provide a better model than presently available for creep analysis of structures under complex mechanical and thermal loading histories.

ACKNOWLEDGEMENTS

This research was supported by Contract No. E(11-1)-2733 of the Energy Research and Development Administration, Washington, D.C., with Cornell University, Ithaca, N.Y. Sincere thanks are expressed to Dr. E.W. Hart of General Electric Co., Schenectady, N.Y. and Professors C.-Y. Li and R.H. Lance of the Cornell Engineering School for valuable discussions regarding Hart's theory.

APPENDIX A

The thermoelastic (zero time) solutions for the problems discussed in Section 3 are [22]

(a) sphere

$$\sigma_r(r,0) = [pa^3(b^3-r^3)+qb^3(r^3-a^3)]/r^3(a^3-b^3)$$

$$+ \alpha E(T_a-T_b)b[1+b-(1+b+b^2)/r+b^2/r^3]/(1-\nu)(b^3-a^3)$$

$$\sigma_\theta(r,0) = [-pa^3(2r^3+b^3)+qb^3(2r^3+a^3)]/2r^3(a^3-b^3)$$

$$+ \alpha E(T_a-T_b)b[1+b-(1+b+b^2)/2r-b^2/2r^3]/(1-\nu)(b^3-a^3)$$

$$T(r) = T_b + (T_a-T_b)\frac{a}{b-a}(\frac{b}{r} - 1)$$

(b) cylinder

$$\sigma_r(r,0) = [pa^2-qb^2-(p-q)a^2b^2/r^2]/(b^2-a^2)$$

$$+ E\alpha[T_bb^2-T_aa^2-(T_b-T_a)a^2b^2/r^2-T(b^2-a^2)]/2(1-\nu)(b^2-a^2)$$

$$\sigma_\theta(r,0) = [pa^2-qb^2+(p-q)a^2b^2/r^2]/(b^2-a^2)+E\alpha[T_bb^2-T_aa^2+(T_b-T_a)a^2b^2/r^2$$

$$-T(b^2-a^2)-(T_b-T_a)(b^2-a^2)/\ell n(b/a)]/2(1-\nu)(b^2-a^2)$$

$$\sigma_z(r,0) = P/\pi(b^2-a^2)+E\alpha[(T_bb^2-T_aa^2)/(b^2-a^2)-(T_b-T_a)/2\ell n(b/a)-T]/(1-\nu)$$

$$T(r) = [T_b\ell n(r/a)+T_a\ell n(b/r)]/\ell n(b/a)$$

(c) rotating disc

$$\sigma_r(r,0) = qb^2(r^2-a^2)/r^2(b^2-a^2)+\rho\omega^2(3+\nu)(a^2+b^2-r^2-a^2b^2/r^2)/8$$

$$+ E\alpha[T_b b^2-T_a a^2-(T_b-T_a)a^2b^2/r^2-T(b^2-a^2)]/2(b^2a^2)$$

$$\sigma_\theta(r,0) = qb^2(r^2+a^2)/r^2(b^2-a^2)+\rho\omega^2[(3+\nu)(a^2+b^2+a^2b^2/r^2)-(1+3\nu)r^2]/8$$

$$+ E\alpha[T_b b^2-T_a a^2+(T_b-T_a)a^2b^2/r^2-T(b^2-a^2)-(T_b-T_a)(b^2-a^2)/\ell n(b/a)]/2(b^2-a^2)$$

Temperature distribution for the disc is the same as for the cylinder.

APPENDIX B

In Section 3b we considered a cylinder with internal and external pressures and axial load. If the end condition is altered and we consider plane strain case instead, $\epsilon_z = 0$. The governing equations remain the same except that 3.14 is dropped. In this case, $\dot{\sigma}_r$ and $\dot{\sigma}_\theta$ are still given by (3.21) and (3.22). However, $\dot{\sigma}_z$ is now given by

$$\dot{\sigma}_z = \frac{E\nu}{(1-\nu^2)}\left\{\int_a^r \frac{(\dot{\epsilon}_r^p-\dot{\epsilon}_\theta^p)}{\eta}\,d\eta - \frac{b^2}{(b^2-a^2)}\int_a^b \frac{(\dot{\epsilon}_r^p-\dot{\epsilon}_\theta^p)}{\eta}\,d\eta\right\}$$

$$- \frac{E\nu(1-2\nu)}{(1-\nu^2)}\frac{1}{(b^2-a^2)}\int_a^b \eta\dot{\epsilon}_z^p d\eta + \frac{E}{(1-\nu^2)}\{\nu\dot{\epsilon}_r^p-(1-\nu)\dot{\epsilon}_z^p\}\ .$$

The initial distribution of σ_z now becomes

$$\sigma_z(r,0) = \nu[\sigma_r(r,0)+\sigma_\theta(r,0)] - E\alpha T(r)$$

where $\sigma_r(r,0)$, $\sigma_\theta(r,0)$ and $T(r)$ are the same as given in Appendix A for the cylinder.

REFERENCES

1. Rabotnov, Y.N., "Creep Problems in Structural Members," North-Holland, Amsterdam, 1969.

2. Penny, R.K., and Marriott, D.L., "Design for Creep," McGraw-Hill, London, 1971.

3. Krempl, E., "The Interaction of Rate and History-dependent Effects and its Significance for Slow Cyclic Inelastic Analysis at Elevated Temperatures," Nuclear Engineering and Desing, Vol. 29, No. 1, Nov. 1974, pp. 125-134.

4. Krempl, E., "Cyclic Creep - an Interpretive Literature Survey," Welding Research Council Bulletin, No. 195, June 1974, pp. 63-123.

5. Krempl, E., "On the Interaction of Rate and History Dependence in Structural Metals", Acta Mechanica, Vol. 22, No. 1-2,1975,pp.53-90.

6. Hart, E.W., "A Phenomenological Theory for Plastic Deformation of Polycrystalline Metals", Acta Metallurgica, Vol. 18, No. 6, June 1970, pp. 599-610.

7. Hart, E.W., Li, C.Y., Yamada, H., and Wire, G.L., "Phenomenological Theory: A Guide to Constitutive Relations and Fundamental Deformation Properties", in "Constitutive Equations in Plasticity," (ed. A.S. Argon), M.I.T. Press, Cambridge, Mass., 1976, pp. 149-197.

8. Hart, E.W., "Constitutive Relations for the Non-Elastic Deformation of Metals", Journal of Engineering Materials and Technology, Trans. ASME, to appear.

9. Miller, A., "An Inelastic Constitutive Model for Monotonic, Cyclic and Creep Deformation: Part I - Equations Developement and Analytical Procedures," paper presented at the Conference on Michromechanical Modelling of Flow and Fracture, Troy, N.Y., June 23-25, 1975 ASME Paper No. 75-Mat-17, Journal of Engineering Materials and Technology, Trans. ASME, to appear.

10. Miller, A., "An Inelastic Constitutive Model for Monotonic, Cyclic and Creep Deformation: Part II - Application to type 304 Stainless Steel," paper presented at the Conference on Michromechanical Modelling of Flow and Fracture, Troy, N.Y., June 23-25, 1975, ASME Paper No. 75-Mat-17, Journal of Engineering Materials and Technology, Trans. ASME, to appear.

11. Lagneborg, R., "A Modified Recovery-Creep Model and Its Evaluation," Metal Science Journal, Vol. 6, July 1972, pp. 127-133.

12. Lee, D., and Hart, E.W., "Stress Relaxation and Mechanical Behavior of Metals," Metallurgical Transactions, Vol. 2, No. 4, Apr. 1971, pp. 1245-1248.

13. Hart, E.W. and Solomon, H.D., "Load Relaxation Studies of Polycrystatline High Purity Aluminum," Acat Metallurgica, Vol. 21, No. 3, Mar. 1973, pp. 295-307.

14. Yamada, H., and Li, C.-Y., "Stress Relaxation and Mechanical Equation of State in Austenitic Stainless Steel," Metallurgical Transactions, Vol. 4, No. 9, Sept. 1973, pp. 2133-2136.

15. Yamada, H., and Li, C.-Y., "Stress Relaxation and Mechanical Equation of State in B.C.C. Metal," Acta Metallurgica, Vol. 22, No. 2, Feb. 1974, pp. 249-253.

16. Yamada, H., and Li, C.-Y., "Stress Relaxation and Mechanical Equation of State in Nickel and T.D. Nickel," presented at the J.E. Dorn Memorial Symposium on "Rate Processes in Plastic Deformation," ASM Fall meeting, 1972.

17. Wire, G.L., Yamada, H., and Li, C.-Y., "Grain Boundary Sliding and Mechanical Equation of State in Lead," Acta Metallurgica, Vol. 22, No. 4, Apr. 1974, pp. 505-512.

18. Wire, G.L., Ellis, F.V., and Li, C.-Y., "Work Hardening and Mechanical Equation of State in Some Metals in Monotonic Loading," Acta Metallurgica, to appear.

19. Ellis, F.V., Wire, G.L., and Li, C.-Y., "Effects of Cold Work and Mechanical Equation of State in 1100 Aluminum Alloy", Journal of Engineering Materials and Technology, Trans. ASME, Vol. 97, No. 4, Oct. 1975, pp. 338-342.

20. Kumar, V., and Mukherjee, S., "Creep Analysis of Structures using a New Equation of State Type Constitutive Relation," Journal of Computers and Structures, to appear.

21. Simmon, G. and Wong, H., "Single Crystal Elastic Constants and Calculated Aggregate Properties," M.I.T. Press, London, 1971.

22. Timoshenko, S.P. and Goodier, J.N., "Theory of Elasticity," 3rd edition, McGraw-Hill, N.Y., 1970.

FIGURE CAPTIONS

Figure 1. Structural elements with loads,
(a) Sphere (a,b) Cylinder (c) Disc

Figure 2. Variation of radial stress in a creeping cylinder, (a) stress redistribution (b) effect of initial hardness on stress relaxation (p = 1000 psi (6.395 M Pa), T_a = 482°F (250°C), T_b = 437°F (225°C), $\kappa = 2$).

Figure 3. Variation of tangential stress in a creeping cylinder.
(a) Stress redistribution (b) Effect of initial hardness on stress relaxation (p = 1000 psi (6.895 M Pa), T_a = 482°F (250°C), T_b = 437°F (225°C), $\kappa = 2$).

Figure 4. Variation of axial stress in a creeping cylinder. (a) Stress redistribution (b) Effect of initial hardness on stress relaxation (p = 1000 psi (6.895 M Pa), T_a = 482°F (250°C), T_b = 437°F (225°C), $\kappa = 2$).

Figure 5. Effect of initial hardness on the relaxation of radial and tangential stresses in a creeping sphere (p = 1500 psi (10.342 M Pa), T_a = 482°F (250°C), T_b = 437°F (225°C), $\kappa = 2$).

Figure 6. Radial displacement at the inner radius of a creeping sphere ($\kappa = 2$) with time for the cases:
(I) p = 3000 psi (20.684 M Pa), $\bar{\sigma}_o^*(\xi)$ = 3.53 (i.e. 10% cold work),
(II) p = 2000 psi (13.790 M Pa), $\bar{\sigma}_o^*(\xi)$ = 5.30 (i.e. 10% cold work),
(III) p = 1500 psi (10.342 M Pa), $\bar{\sigma}_o^*(\xi) = 2.0\ \bar{\sigma}(\xi,0)$,
(IV) p = 1500 psi (10.342 M Pa), $\bar{\sigma}_o^*(\xi)$ = 7.07 (i.e. 10% cold work),
T_a = 482°F (250°C) , T_b = 437°F (225°C).

Figure 7. Growth of hardness with time at $\xi = 1.3$ in a creeping sphere (p = 1500psi (10.342 M Pa), T_a = 482°F (250°C), T_b = 437°F (225°C), $\kappa = 2$).

Figure 8. Redistribution of radial stress in a rotating disc under creep (N = 10,000 rpm (ω = 1047.2 rad/s), $\bar{\sigma}_o^*(\xi)$ = 38.14 (i.e. 10% cold work), $\kappa = 3$, a = 1 in.(2.54 cm)).
(a) T_a = 482°F (250°C), T_b = 437°F (225°C)
(b) $T_a = T_b$ = 482°F.

Figure 9. Redistribution of tangential stress in a rotating discunder creep (N = 10,000 rpm (ω = 1047.2 rad/s), $\bar{\sigma}_o^*(\xi)$ = 38.14 (i.e. 10% cold work), κ = 3, a = 1 in.(2.54 cm)).
(a) T_a = 482°F (250°C), T_b = 437°F (225°C)
(b) $T_a = T_b$ = 482°F.

Figure 10. Radial displacement and thickness change at the inner and outer radii of a rotating disc under creep (N = 10,000 rpm (ω = 1047.2 rad/s), $\bar{\sigma}_o^*(\xi)$ = 38.14 (i.e. 10% cold work), T_a = 482°F (250°C), T_b = 437°F (225°C), κ = 3, a = 1 in.(2.54 cm)).

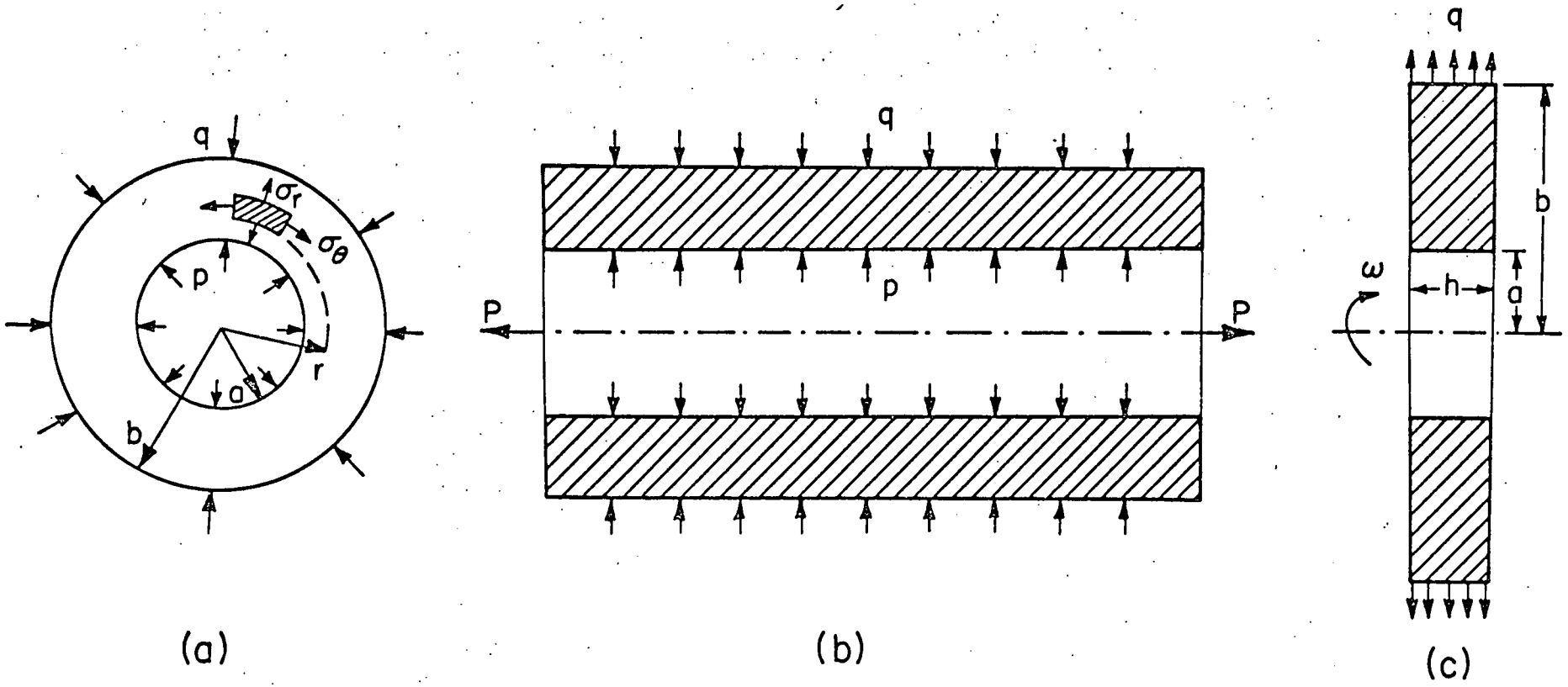

Figure 1. Structural elements with loads,

(a) Sphere (a,b) Cylinder (c) Disc

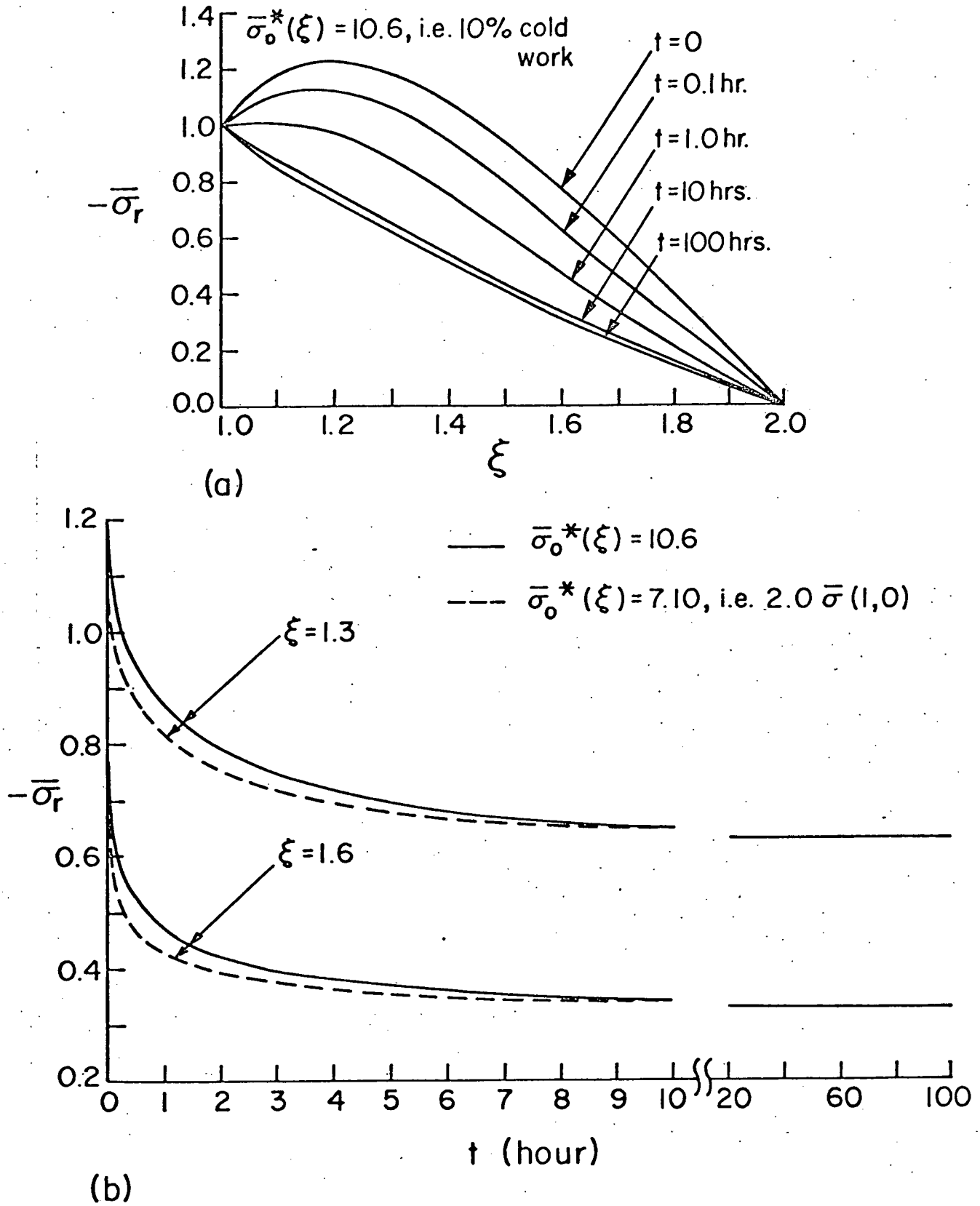

Figure 2. Variation of radial stress in a creeping cylinder, (a) stress redistribution (b) effect of initial hardness on stress relaxation (p = 1000 psi (6.395 M Pa), T_a = 482°F (250°C), T_b = 437°F (225°C), κ = 2).

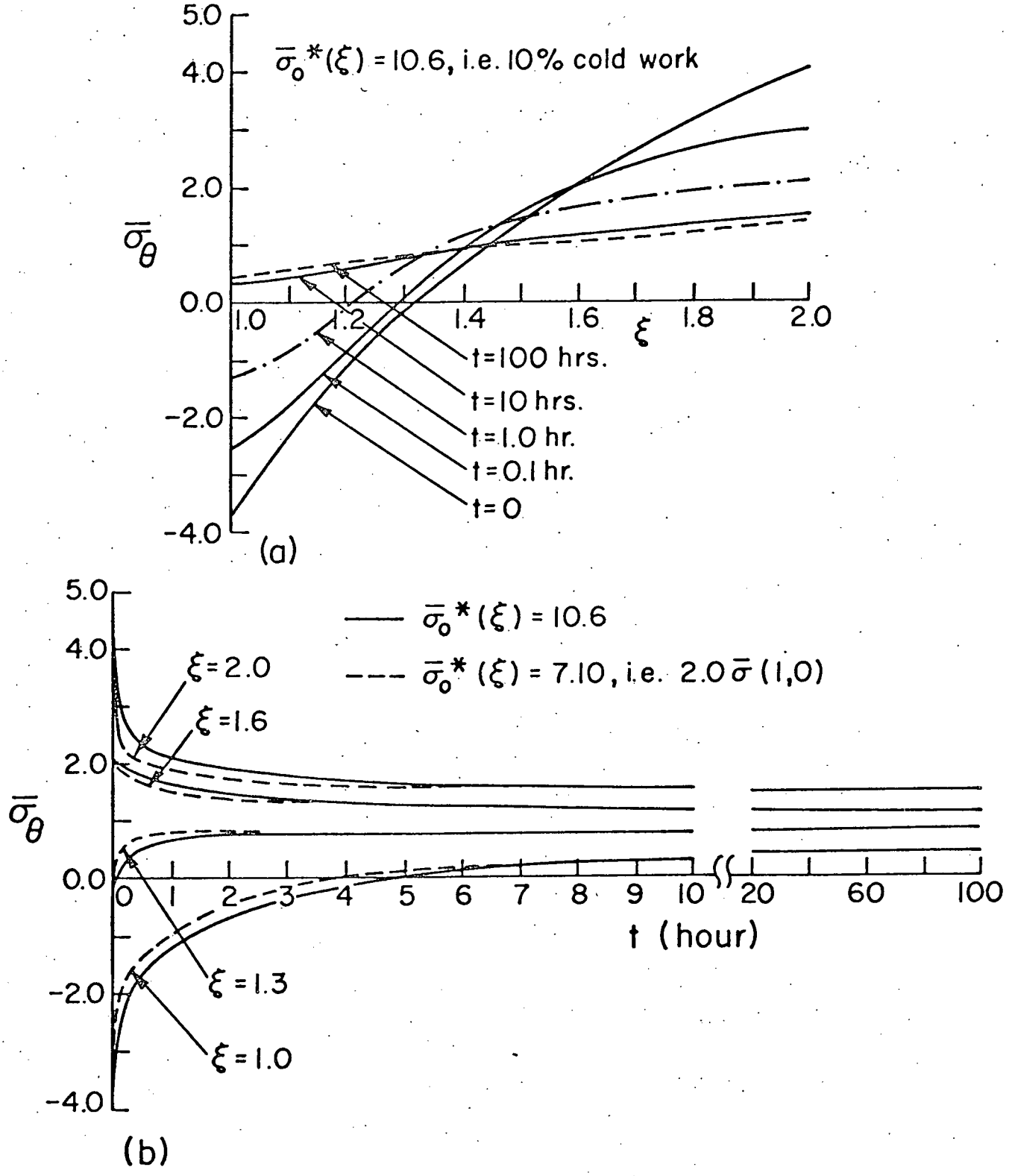

Figure 3. Variation of tangential stress in a creeping cylinder. (a) Stress redistribution (b) Effect of initial hardness on stress relaxation (p = 1000 psi (6.895 M Pa), T_a = 482°F (250°C), T_b = 437°F (225°C); κ = 2).

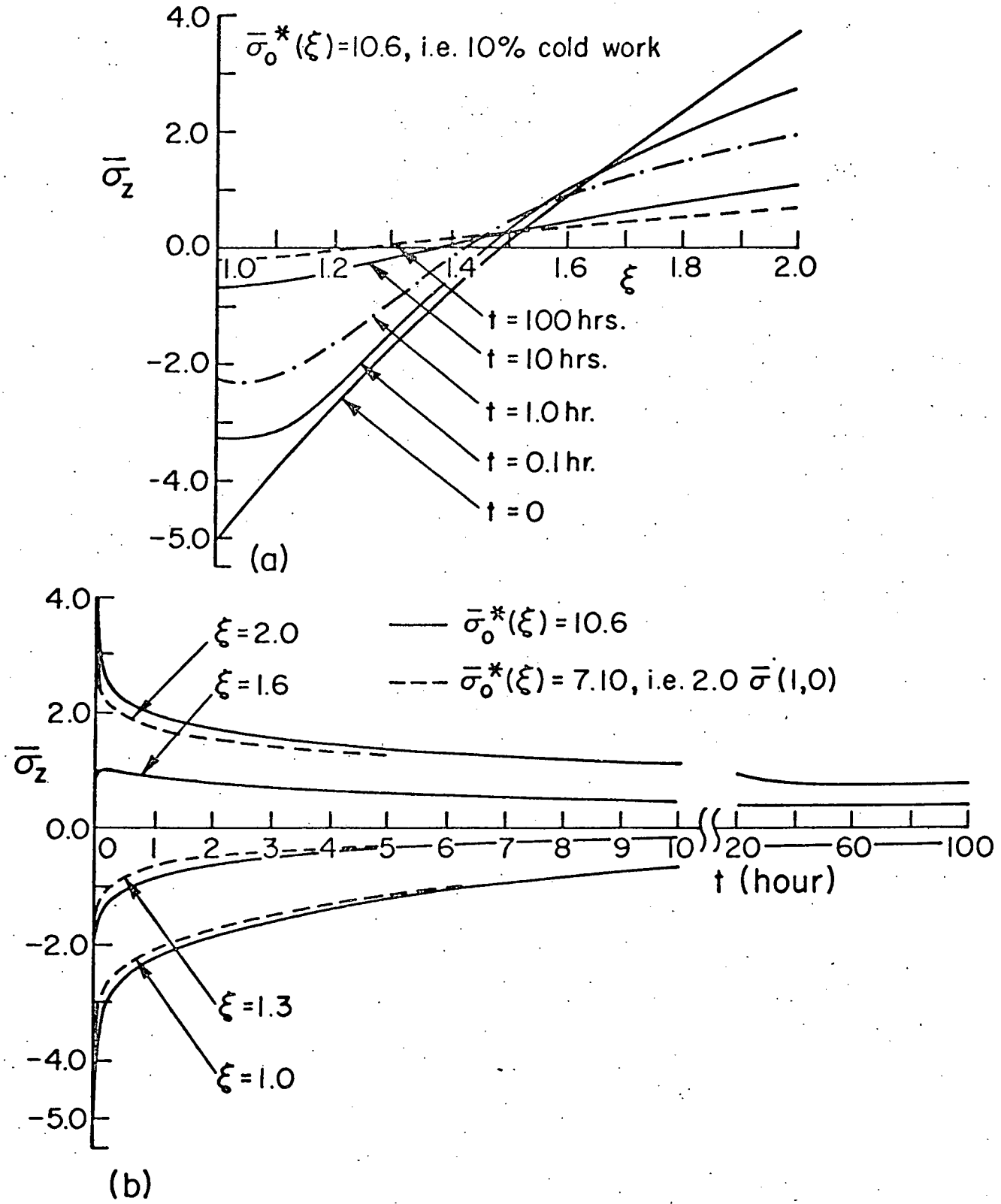

Figure 4. Variation of axial stress in a creeping cylinder. (a) Stress redistribution (b) Effect of initial hardness on stress relaxation (p = 1000 psi (6.895 M Pa), T_a = 482°F (250°C), T_b = 437°F (225°C), κ = 2).

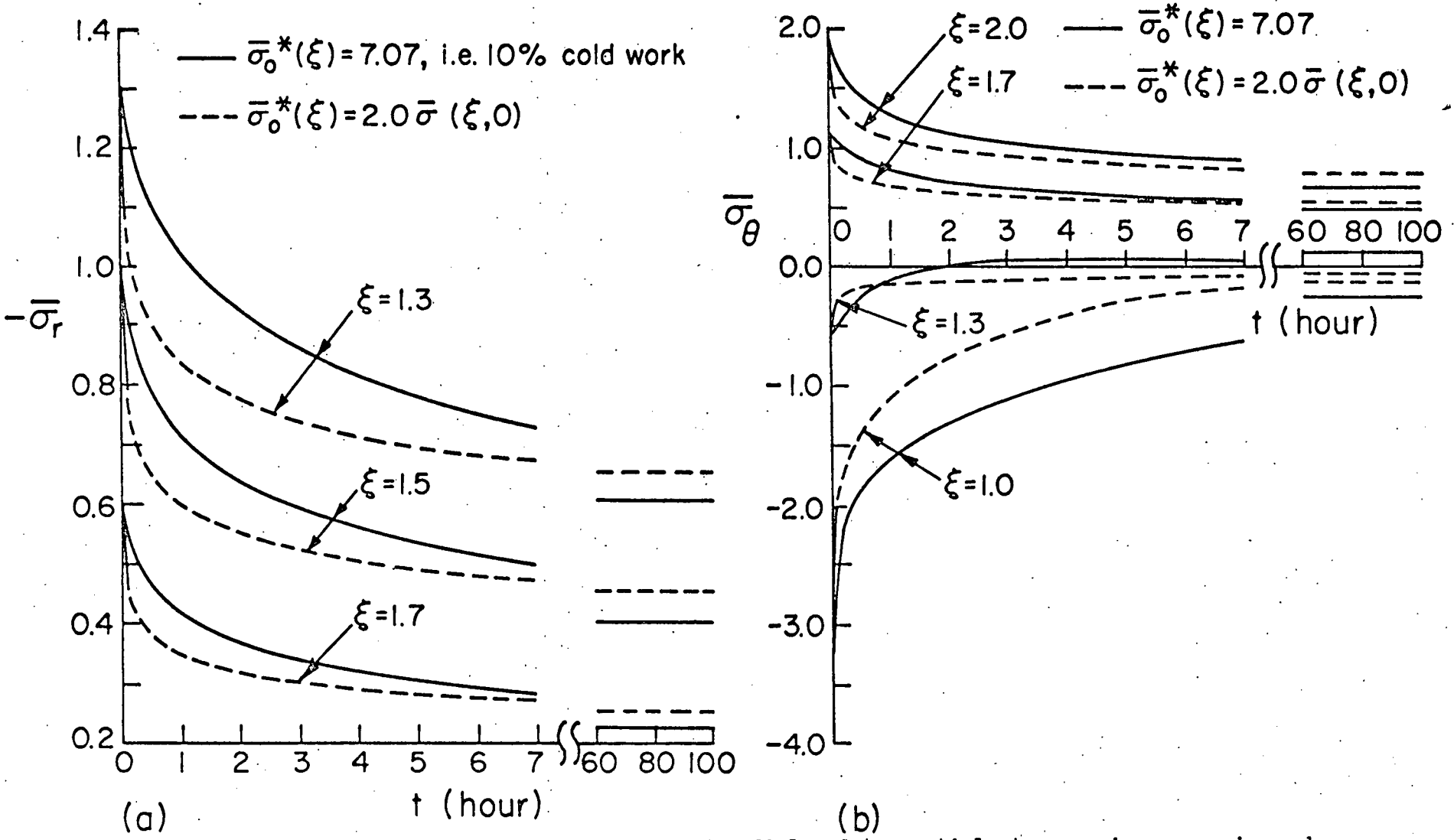

Figure 5. Effect of initial hardness on the relaxation of radial and tangential stresses in a creeping sphere (p = 1500 psi (10.342 M Pa), T_a = 482°F (250°C), T_b = 437°F (225°C), κ = 2).

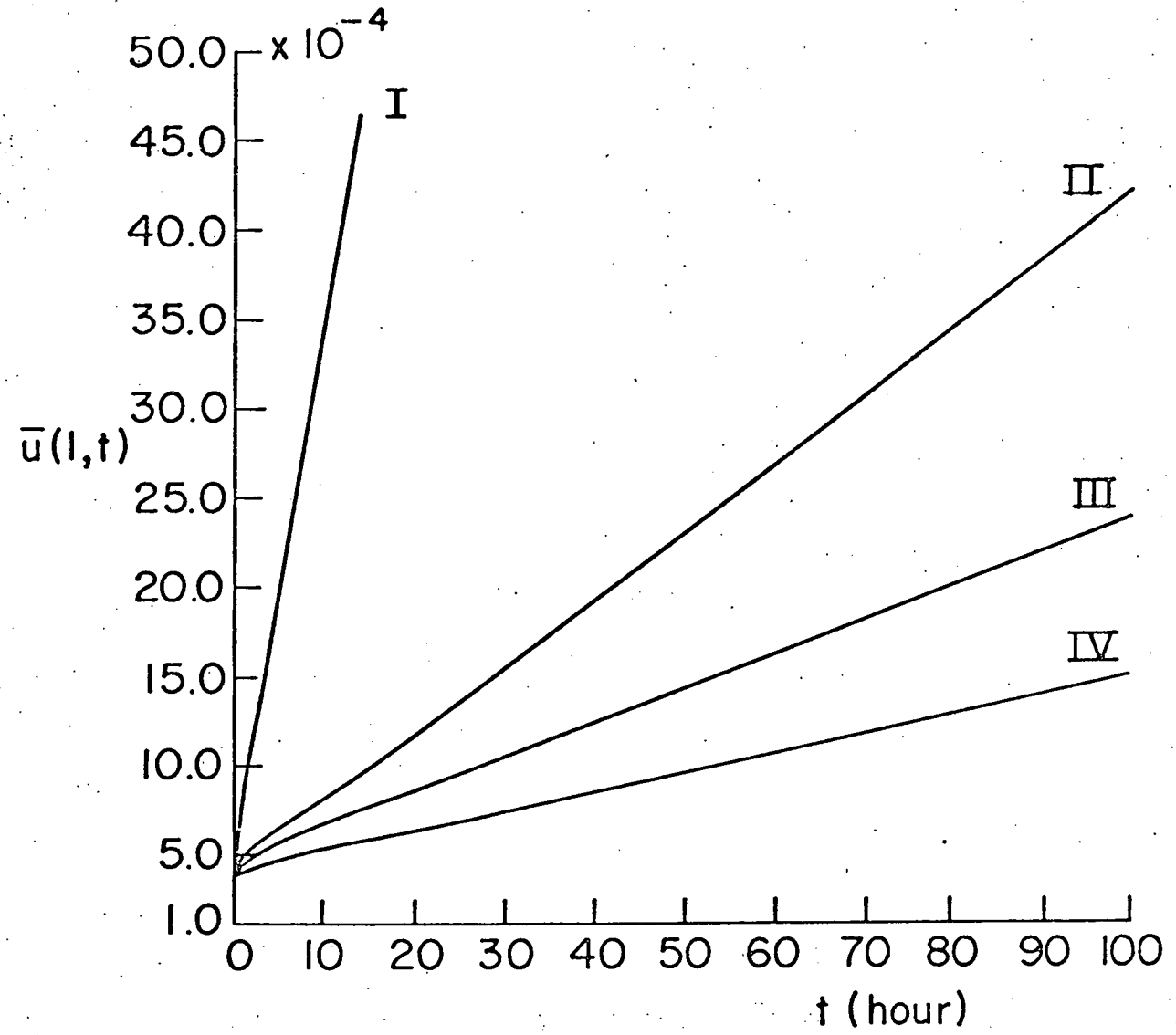

Figure 6. Radial displacement at the inner radius of a creeping sphere ($\kappa = 2$) with time for the cases:

(I) p = 3000 psi (20.684 M Pa), $\bar{\sigma}_o^*(\xi) = 3.53$ (i.e. 10% cold work),

(II) p = 2000 psi (13.790 M Pa), $\bar{\sigma}_o^*(\xi) = 5.30$ (i.e. 10% cold work),

(III) p = 1500 psi (10.342 M Pa), $\bar{\sigma}_o^*(\xi) = 2.0\ \bar{\sigma}(\xi,0)$,

(IV) p = 1500 psi (10.342 M Pa), $\bar{\sigma}_o^*(\xi) = 7.07$ (i.e. 10% cold work),

$T_a = 482°F$ (250°C) , $T_b = 437°F$ (225°C).

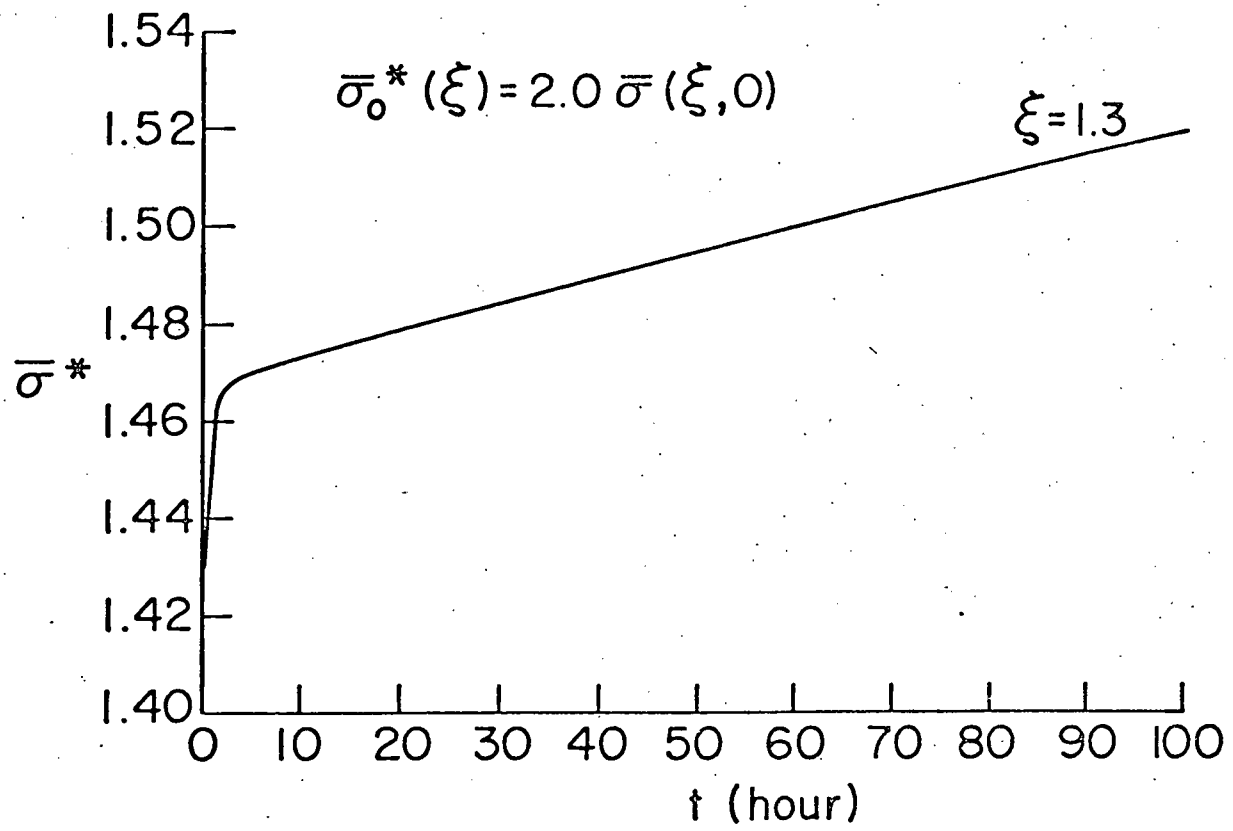

Figure 7. Growth of hardness with time at $\xi = 1.3$ in a creeping sphere (p = 1500 psi (10.342 M Pa), T_a = 482°F (250°C), T_b = 437°F (225°C), $\kappa = 2$).

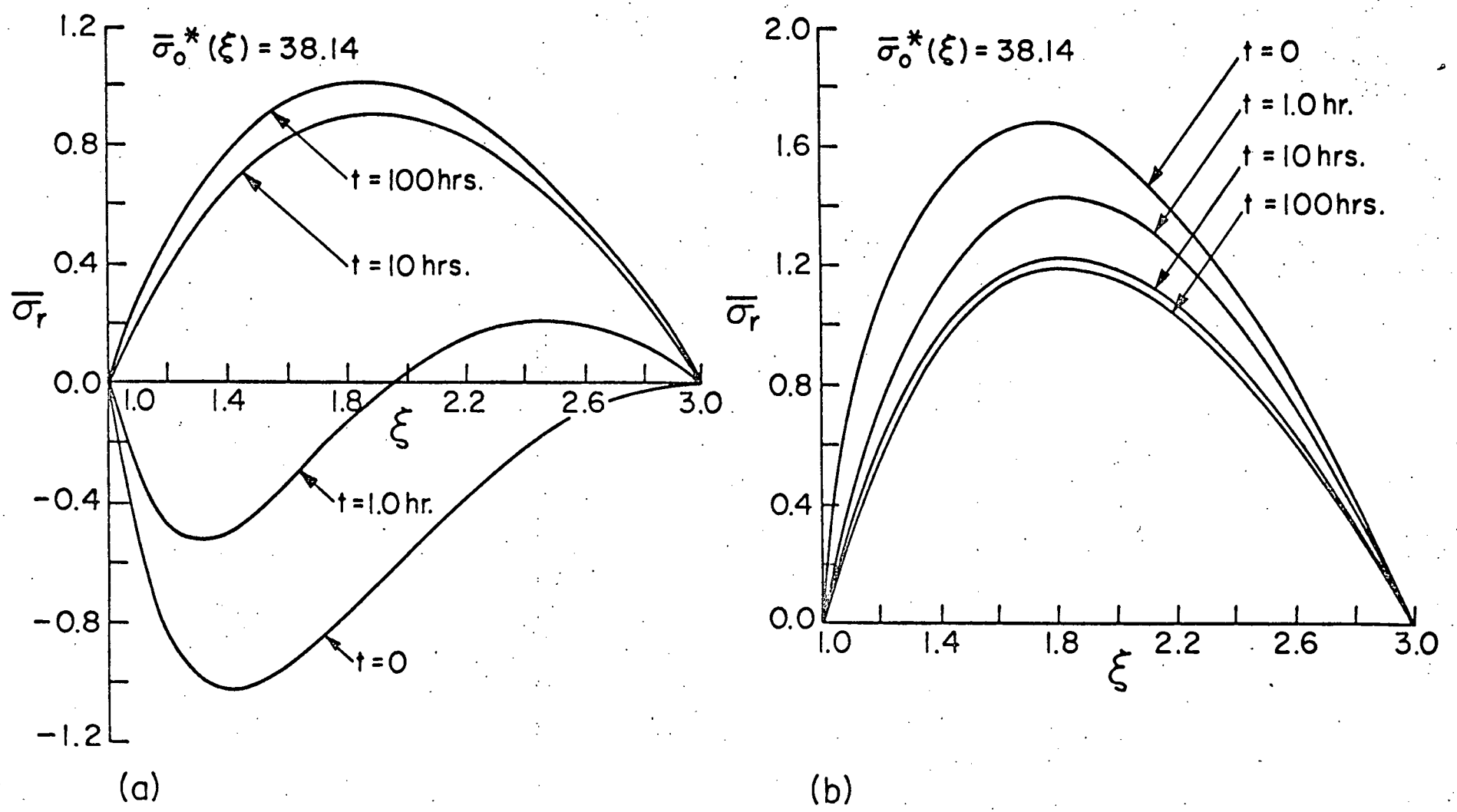

Figure 8. Redistribution of radial stress in a rotating disc under creep (N = 10,000 rpm (ω = 1047.2 rad/s), $\bar{\sigma}_o^*(\xi)$ = 38.14 (i.e. 10% cold work), κ = 3, a = 1 in.(2.54 cm)).
(a) T_a = 482°F (250°), T_b =437°F (225°C) (b) $T_a = T_b$ = 482°F.

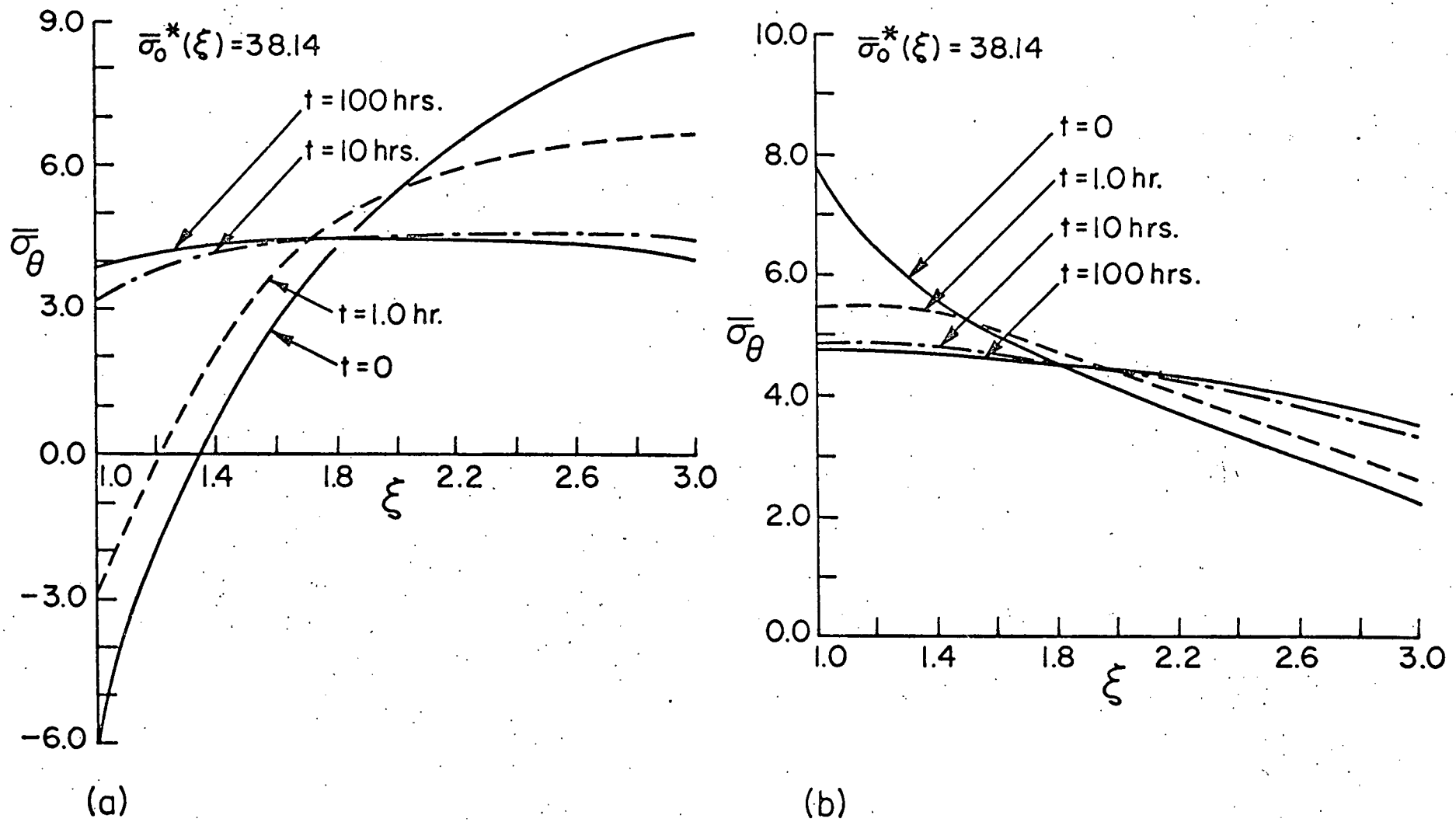

Figure 9. Redistribution of tangential stress in a rotating disc under creep (N = 10,000 rpm (ω = 1047.2 rad/s), $\bar{\sigma}_o^*(\xi)$ = 38.14 (i.e. 10% cold work), κ = 3, a = 1 in. (2.54 cm)).
(a) T_a = 482°F (250°C), T_b = 437°F (225°C) (b) $T_a = T_b$ = 482°F.

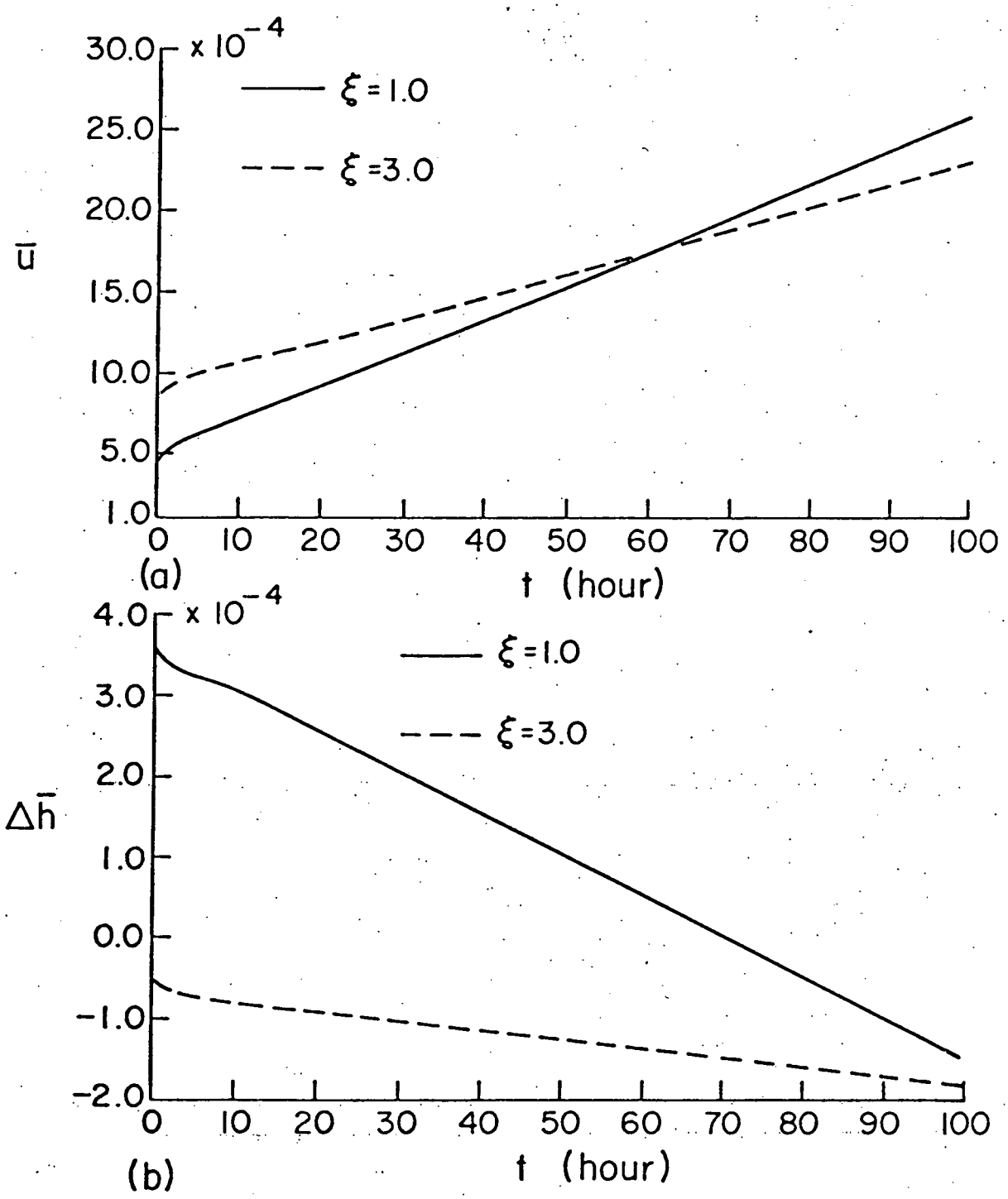

Figure 10. Radial displacement and thickness change at the inner and outer radii of a rotating disc under creep (N = 10,000 rpm (ω = 1047.2 rad/s), $\bar{\sigma}^{*}(\xi)$ = 38.14 (i.e. 10% cold work), T_a = 482°F (250°C), T_b^o = 437°F (225°C), κ = 3, a = 1 in.(2.54 cm)).